Methane combustion in various regimes: First and second thermodynamic-law comparison between air-firing and oxyfuel condition

Yaming Liu [1], Sheng Chen *[2,3,4], Shi Liu [1],

Yongxin Feng [1], Kai Xu [1], Chuguang Zheng [2]

1. Electric Power Research Institute of Guangdong Power Grid Company, Guangzhou 510080, China

2. State Key Laboratory of Coal Combustion, Huazhong University of Science and Technology, Wuhan 430074, China

3. Institute for Modelling and Simulation in Fluodynamics, Nanoscience and Industrial Mathematics "Gregorio Millán Barbany", Universidad Carlos III de Madrid, Leganes 28911, Spain

4. Faculty of Engineering, The University of Nottingham, University Park, Nottingham NG7 2RD, UK

* *Corresponding author. Faculty of Engineering, University of Nottingham. E-mail address: shengchen.hust@gmail.com (Sheng Chen)*

Abstract

MILD oxyfuel combustion has been attracting increasing attention as a promising clean combustion technology. How to design a pathway to reach MILD oxyfuel combustion regime and what can provide a theoretical guide to design such a pathway are two critical questions that need to be answered. So far there has been no open literature on these issues. A type of combustion regime classification map proposed in our previous work, based on the so-called "Hot Diluted Diffusion Ignition" (HDDI) configuration, is adopted here as a simple but useful tool to solve these problems. Firstly, we analyze comprehensively the influences of various dilution atmosphere and fuel type on combustion regimes. The combustion regime classification maps are made out according to the analyses. In succession, we conduct a comparison between the map in air-firing condition and its oxyfuel counterpart. With the aid of the second thermodynamic-law analysis on the maps, it is easy to identify the major contributors to entropy generation in various combustion regimes in advance, which is crucial for com-

bustion system optimization. Moreover, we find that, for the first time, a combustion regime classification map also may be used as a safety indicator. With the aid of these maps, some conclusions in previous publications can be explained more straightforwardly.

Keywords:

MILD combustion; oxyfuel combustion; counter flow combustion; entropy generation

1 Introduction

Although industrial and academic communities always pursue to develop a more efficient way to generate heat and power, combustion is still playing a predominant role in energy conversion of most daily and industrial applications, not only in current stage but also in the visible future [1]. Combustion usually faces two main challenges: (1) to improve the efficiency of combustion processes and (2) to reduce air pollutant products by combustion processes. The former is extremely important for industries as it

contributes to their operational costs while the public pays high attention on the latter as it concerns our well-being. Unfortunately, there is a tradeoff between these two respects as in general it is difficult to eliminate air pollution while maintaining a high combustion efficiency. To overcome this difficulty, some innovative combustion technologies are inspired recently. Among them, two, namely MILD (Moderate or Intense Low oxygen Dilution) combustion [2] and oxyfuel combustion [3], attract increasing attention.

Compared with the conventional combustion technologies, MILD combustion is a type of "slow" reaction as the reactants are diluted to moderate the oxidization rates of fuels. Consequently, the peak temperature of combustion will decrease and the temperature distribution will become even, which can eliminate thermal NO_x production effectively [2]. Meanwhile, it was found that unburnt hydrocarbon products also could be reduced significantly by MILD combustion [4]. It is an interesting feature as few available combustion technologies can satisfy, simultaneously, the re-

quirements of low NO_x emission and low unburnt hydrocarbon production. More excitingly, it was observed that fuel nitrogen translation also could be suppressed in MILD condition [5]. Due to its intrinsic advantages, MILD combustion is regarded as a promising clean combustion technology in this century [2]. Until now, numerous research has been published on MILD combustion. The majority of them may fall into five categories. The first one tries to classify different combustion regimes by a map, which can straightforwardly illustrate the relationship between various combustion regimes. De Joannon et al. discussed how to classify combustion regimes in a number of different combustion configurations [6–8]. In their work the influences of various combustion pressures were also investigated. In order to classify combustion regimes more conveniently, some of the present authors[9] proposed to adopt the effective equivalence ratio of reactants and the temperature of oxidant flow as the coordinate axes, instead of those used in Refs.[6,7], to plot the map, as these two parameters can be obtained directly from practical combustion system-

s. The above studies all are based on the so-called counter-flow combustion configuration. Recently, Wang et al. [10] investigated the combustion regimes of a co-flow configuration. They observed that in co-flow combustion there was a quasi-MILD regime which was similar with MILD combustion but did not share the same features of MILD combustion. More recently, Evans et al. [11] proposed a new approach, based on the initial/final temperature and the effective activation energy of reaction, to classify combustion regimes. Their effort provided an insight into classification of different types of combustion. The second category focuses on the special reaction structures of MILD combustion. Szego et al. [12] reported the profiles of temperature and concentration inside a lab-scale furnace operated in MILD combustion condition. Their work paid high attention on how to form MILD combustion stably. A so-called jet in hot coflow (JHC) burner was designed in Ref.[13]. The temporally and spatially resolved measurements of reactive scalars were carried out with the aid of this equipment. As it can prevent atmosphere to affect the fine reaction structures

of MILD combustion within the core zone, the JHC burner has been widely used in the MILD combustion research community, especially for MILD combustion simulation. The influences of different fuels on reaction structures of MILD combustion also have been reported [14,15]. It was found that MILD combustion was highly flexible to various fuels. As MILD combustion is a kind of "bulk" combustion, therefore the furnace chamber shape would influence MILD combustion more significantly, as compared with traditional combustion modes. Recently some of the present authors discussed such topic[16]. The results demonstrated that a larger divergence angle of a furnace would be better to establish MILD combustion. The publications on reaction structures of MILD combustion are too many to be listed here. A detailed review on it has been presented in Refs.[2,17]. The efforts on simplified reaction mechanisms of MILD combustion constitute the third category, which is indispensable for industrial-scale simulation. Kim et al.[18] compared different global reaction mechanisms for MILD combustion simulation. As their study was based

on the so-called "Sandia Flame-D" which is not a typical MILD combustion research prototype, the conclusions drawn in Ref.[18] were questionable. Some of the present authors also made an comprehensive comparison between several popularly used global reaction mechanisms, with the aid of the JHC configuration [19]. It was observed that these global reaction mechanisms all could predict the major concentrations sufficiently accurately, except carbon monoxide. Based on the analyses, the same authors proposed a new global reaction mechanism for MILD combustion research [20]. Compared against the GRI-Mech3.0, Hamdi et al.[21] proposed a 5-step and a 9-step reduced reaction mechanism for natural gas MILD combustion simulation. They claimed that the latter was better for NO_x and CO prediction. Nitrogen translation pathways in MILD combustion condition were also investigated[22–26]. Some studies revealed that the NNH and N_2O routes were the most important pathways in NO formation in MILD condition [27–31]. The next category covers the aerodynamics of MILD combustion. Historically, MILD combustion

can be looked as a variant of High Temperature Air Combustion (HiTAC)[2]. Consequently, in the early stage of MILD combustion research, preheating of reactants was regarded as one of the necessary conditions to establish MILD combustion. Later, it was found that aerodynamics played a predominant role on sustaining MILD combustion and a MILD regime might be formed in a furnace even without preheating [32]. In succession, it was reported, compared with traditional combustion modes, molecular diffusion could not be ignored in the MILD combustion regime investigated in Ref.[33]. The latest research concentrates in the effect of aerodynamics on reaction rates of fuels in MILD regime, namely the so-called turbulence-chemistry interaction [34,35], as it has been widely accepted that most popularly used models for turbulence-chemistry interaction were not suitable for MILD combustion simulation [9]. The above research all are based on the first thermodynamic-law analysis. Recently, a number of studies starting from the second thermodynamic-law begin to emerge. In this paper they are classified as the last category. In Ref.[36]

it was revealed that the exergy efficiency of a lab-scale furnace operated in MILD combustion regime is significantly higher than that under conventional combustion conditions. The same authors showed this conclusion could hold water for different fuels[37]. A comparison of entropy generation between different combustion regimes was made by the present authors [9]. It was observed that the maximum exergy loss in hydrogen-air MILD combustion regime depended closely on a number of operational parameters.

At first, the oxyfuel combustion technology was developed to address the global warming challenge due to the intensive man-made CO_2 emissions[3,38]. Soon, it was observed that some air pollutant products also could be suppressed in oxyfuel condition [39]. Numerous studies have been published during the past decades on different aspects of oxyfuel combustion, such as burner design [40,41], reaction mechanisms [42,43], techno-economic assessment[44,45] and so on. A number of review papers are also available[39,46,47]. A latest review on numerical modeling of oxy-

fuel combustion is presented in Ref.[48]. The oxyfuel combustion technology is regarded as one of the most promising options in the near future to restrict CO_2 concentration in the atmosphere [3]. Until now, some pilot-scale demonstrations have been built up and a number of commercial-scale units are under consideration [49].

To remedy some shortcomings of the "standard" oxyfuel combustion technology, recently a so-called MILD oxyfuel conception was proposed [20,50–53]. The MILD oxyfuel combustion is an organic combination of MILD and oxyfuel technologies, namely to establish and sustain a MILD combustion regime in CO_2/O_2 atmosphere [20]. Originally, the present authors proposed this new conception to utilize biogas with a higher efficiency[20,51]. Later, it was extended to different fuels [50,52,53]. The fine structures of MILD oxyfuel combustion have been investigated with the aid of numerical simulation [20,51–53] and its feasibility has also been proven by experimental studies [50]. However, as a recently emerging research area, a lot of efforts are still required to deepen

our insight into it. For example, from the viewpoint of industrial practice, it is impossible to reach a MILD oxyfuel regime directly. According to our experimental experience, a safe pathway to establish and sustain a MILD oxyfuel regime in a furnace may be: air-firing $\rightarrow$ oxyfuel combustion $\rightarrow$ MILD oxyfuel regime [54]. However, how to design a safe and effective transition pathway is still an open question. More important, we should answer what can be used as a theoretical guide to design such a transition pathway for practical applications. Unfortunately until now nobody has focused on these critical problems. After a careful consideration, a type of map on combustion regime classification, which was proposed in our recent investigation [9], may provide an appropriate option to solve these problems. Therefore, maps to classify various combustion regimes in air-firing and oxyfuel condition, besides a comparison between these maps, are extremely necessary. With such combustion regime classification maps and related comparison, we may further optimize the transition pathways for practical operation in advance. But surprisingly, to the

best knowledge of the present authors, nowadays there is no open literature on it. As mentioned above, until now there have been only a number of studies on combustion regime classification in air-firing condition. Such gap inspires the present work.

The main originalities of the present work is fourfold: (1) For the first time, we analyze comprehensively the influences of different dilution atmosphere on combustion regimes. According to the analyses, the combustion regime classification maps are made out. (2) In succession we make a comparison between the map in air-firing condition and its oxyfuel counterpart, not only from the viewpoint of the first thermodynamic-law but also from that of the second thermodynamic-law. The comparison provides a consistent solution to the above problems with a solid theoretical base. (3) With the aid of the second thermodynamic-law analysis on the maps, it is easy to identify the major contributors to entropy generation in various combustion regimes in advance, which is crucial for combustion system optimization. (4) Through the comparison between different fuels, we find that, for the first time,

a combustion regime classification map can be used as a safety indicator for practical operation. Such exciting finding can extensively expand the purposes of a combustion regime classification map. Moreover, with the aid of these maps, some conclusions in previous publications can be explained more straightforwardly. Meanwhile, a new question is arisen: whether the conclusions in the present work can be extended for other fuels. It will be answered by our future work.

2 Specification of the problem and mathematical modeling

The so-called "Hot Diluted Diffusion Ignition" (HDDI) configuration is adopted in the present work as it is a popularly used research prototype to classify combustion regimes [7]. Such configuration is composed by two opposed jets: one jet for oxidant flow and the other for fuel flow, as illustrated by Fig.1. The aspect ratio of the investigated domain is $A = \frac{L}{W} = 0.6$, where W is the diameter of jets and the distance between the jets is $2L$. In this figure, the boundary conditions are also given, the same as

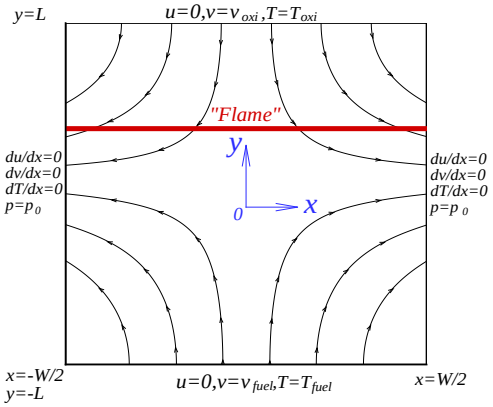

Fig. 1. Schematic configuration and coordinate system of the computational domain adopted in our previous work [9,20,51].

that in our previous work [9,20,51]. Two-dimensional rectangular coordinates are used. The origin of the coordinates is located at the domain geometric center. Fuel flow (CH_4/CO_2 in oxyfuel operation and CH_4/N_2 in air-firing operation), is uniformly ejected from the bottom wall with velocity $v = v_{fuel}$ and temperature $T_{fuel} = T_0$, where T_0 is the atmosphere temperature. The pre-heated oxygen (diluted by CO_2 in oxyfuel operation and N_2 in air-firing operation), is uniformly ejected from the top wall with velocity $v = v_{oxi}$ and temperature T_{oxi}. The counter flow impacts and reacts in the reaction zone. Then, a diffusion stagnation "flame" is formed.

The dimensionless governing equations in Cartesian coordinates

for such laminar steady reacting flows have been given in our previous studies [51], which read

$$\partial_t \rho + \nabla_\alpha \rho u_\alpha = 0, \tag{1}$$

$$\partial_t \rho u_\alpha + \nabla_\beta \rho u_\alpha u_\beta = -\nabla_\alpha P + \frac{1}{Re} \nabla_\beta \mu (\nabla_\alpha u_\beta + \nabla_\beta u_\alpha), \tag{2}$$

$$\partial_t T + u_\alpha \nabla_\alpha T = \frac{1}{\rho Re Pr} \nabla_\alpha \mu \nabla_\alpha T + \sum_{i=1}^{N} h_i \omega_i, \tag{3}$$

$$\partial_t Y_i + u_\alpha \nabla_\alpha Y_i = \frac{1}{\rho Re Sc} \nabla_\alpha \mu \nabla_\alpha Y_i + \omega_i, \tag{4}$$

$$\rho = \frac{\overline{W}}{RT}. \tag{5}$$

where $Re = \rho_0 u_0 L_0/\mu_0$, $Pr = \mu Cp/(\rho\kappa)$ and $Sc = \mu/(\rho D_i)$ are the Reynolds, Prandtl and Schmidt numbers respectively. The variables, such as density ρ, velocity u_α, temperature T and total pressure P, are normalized by the reference values of density ρ_0, velocity u_0, temperature T_0, length L_0, static pressure p_0 and dynamic viscosity μ_0. The detailed normalized process can be found in [20,51]. $\overline{W}$ is the mean molecular weight of the mixture and Cp is the specific heat capacity of the reactants[55]. The above governing equations are derived under the low Mach number as-

sumption together with the following premises: (1) There are no external forces; (2) The diffusion obeys the Fick's law of diffusion; (3) Viscous energy dissipation is neglected. The subscripts α and β in the above equations represent Cartesian coordinates and the summation convention is applied to these subscripts. The heat inter-diffusion term does not appear in the above equations because the terms of second order and above in the Mach number have been neglected under the low Mach number approximation [55].

The inlet Reynolds number is defined as[51]

$$Re = \frac{v_{air} L}{\nu_{air}}, \tag{6}$$

where ν_{air} is the kinematic viscosity of air. The velocity v_{fuel} is determined by

$$Re = \frac{v_{fuel} L}{\nu_{fuel}}, \tag{7}$$

where ν_{fuel} is the kinematic viscosity of fuel mixture and $2L$ is the distance between the opposed jets. In the present work, the

Reynolds numbers of both jet flow are identical as $Re = 100$ and a simple lattice Boltzmann apporach proposed in our previous research [55] is used to solve the above governing equations. The thermodynamic and transport properties appearing in the governing equations are given in our previous work [43]. The reaction kinetic mechanisms used in our previous studies [43,20] are adopted here again, as shown below:

$$CH_4 + 1.5O_2 \rightarrow CO + 2H_2O \tag{8}$$

$$CO + 0.5O_2 \rightleftharpoons CO_2 \tag{9}$$

$$H_2 + 0.5O_2 \rightleftharpoons H_2O \tag{10}$$

$$\omega_{ov} = k_{ov} T^{\beta} \prod_{j=1}^{N} (\frac{\rho Y_j}{W_j})^{\alpha_j} \exp(-E/RT) \tag{11}$$

where β is the temperature exponent, ω_{ov} is the over-all reaction

Table 1
Global combustion mechanisms with kinetic rate data (unit in kmol, m^3, K, s, KJ).

Reaction mechanism	Rate orders	β	k_{ov}	E/R
(R1) $CH_4 + 1.5O_2 \rightarrow CO + 2H_2O$	$[CH_4]^{0.7}[O_2]^{0.8}$	0	5.03×10^{11}	24056
(R2) $CO + 0.5O_2 \rightharpoonup CO_2$	$[CO][H_2O]^{0.5}[O_2]^{0.25}$	0	2.24×10^{8}	5032
(R3) $CO_2 \rightharpoonup CO + 0.5O_2$	$[CO_2][H_2O]^{0.5}[O_2]^{-0.25}$	-0.97	1.10×10^{13}	39452
(R4) $H_2O \rightharpoonup H_2 + 0.5O_2$	$[H_2O]$	0	3.48×10^{13}	47907
(R5) $H_2 + 0.5O_2 \rightharpoonup H_2O$	$[H_2][O_2]^{0.5}$	0	7.91×10^{10}	17609

rate, k_{ov} is the reaction coefficient, E is the effective activation energy, R is the universal gas constant and α_j, Y_j and W_j are the reaction exponent, mass fraction and molecular weight of the j-th reactant. The corresponding reaction rate data in these global chemical reaction mechanisms are given in Table 1.

3 The entropy generation equation

As mentioned above, the flow field and the distribution of scalar properties, such as temperature and species mass fractions, are obtained from numerical solution of the above governing equations. From the flow and scalar field distributions, the local entropy generation number can be computed using the entropy gen-

eration equation, which is obtained in the following form[51]:

$$S = \frac{\prod : \nabla \vec{u}}{T} + \frac{k \nabla T \cdot \nabla T}{T^2} + \sum_i \frac{\rho D_i}{x_i} \nabla y_i \cdot \nabla x_i - \sum_i \frac{\mu_i \omega_i}{T} \quad (12)$$

What should be accentuated is that Eq.(12) adopted in the present work is also dimensionless. The first term on the right-hand side of Eq. (12) is due to fluid friction (referred to as S_{vis}), the second term is due to heat transfer (referred to as S_{cond}), the third term pertains to mass transfer (referred to as S_{mix}) and the fourth term is due to chemical reaction (referred to as S_{chem}). The last two terms have summation over all the species and for all the reactions. Because there is no external body force in the present situation, the entropy generation induced by body force vanishes in Eq. (12). The entropy generation term due to coupling between heat and mass transfer also can be ignored in the above equation since it usually makes rare contribution to the local entropy generation rate unless the Soret and Dufour effects have significant influence[56]. In Eq. (12), $\prod$ is the viscous stress, $\vec{u}$ is the velocity vector, ρ is the density of the mixture and k is the thermal

conductivity. y_i, x_i, ω_i, D_i and μ_i are the mass fraction, the mole fraction, the production rate, diffusion coefficient and chemical potential of species i respectively. The total entropy generation number is defined as[51]

$$S_{total} = \int_{\Omega} S \partial \Omega \tag{13}$$

where Ω means the global computational domain. Similar expressions can be written for $S_{vis,total}$, $S_{cond,total}$, $S_{mix,total}$ and $S_{chem,total}$. The relative total entropy generation rates due to heat transfer, chemical reaction, fluid friction and mixing are defined as $\gamma_{cond,total} = S_{cond,total}/S_{total}$, $\gamma_{chem,total} = S_{chem,total}/S_{total}$, $\gamma_{vis,total} = S_{vis,total}/S_{total}$ and $\gamma_{mix,total} = S_{mix,total}/S_{total}$ [56].

4 Results and discussions

The grid resolution used in this work is 300×180. It has been demonstrated in our previous studies [9,20,51] that such grid resolution is fine enough for the present investigated domain. The

validation of our computer programme code has been presented in detail in our previous publications [9,20,51,55,56]. The equivalence ratio φ and the temperature of oxidant flow T_{oxi} are adopted here as the arguments to classify different combustion regimes. As demonstrated in our previous work [9], these two parameters can be available straightforwardly in practical applications. In the present investigation, the variable range of φ is very wide, from the highly diluted fuel region ($\varphi < 0.5$) to the fuel-rich region ($\varphi = 1.4$) and T_{oxi}/T_0 varies from 1.0 to 6.0. What should be emphasized is that for $T_{oxi}/T_0 = 1.0$, a temporary high temperature source is required to ignite the reactants, the same as that in our previous studies [20,55].

4.1 Influences of fuel type and dilution atmosphere on combustion regimes

In this subsection, the influences of different fuels and dilution atmosphere on combustion regimes are discussed. The influences of fuels on combustion regimes are revealed through a comparison between methane and hydrogen in air-firing condition while

methane HDDI combustion in air and CO_2/O_2 (oxyfuel) atmosphere are chosen to show the influences of dilution atmosphere on combustion regimes.

4.1.1 Temperature profiles in air-firing condition and comparison between different fuels

Figure 2 illustrates the temperature profiles of methane-air HDDI combustion at various equivalence ratio and preheating temperature of oxidant flow, where $\varphi = 0.5$ (critical point of ultra-lean/highly diluted fuel region), $\varphi = 0.7$ (critical point of ultra-lean/lean fuel region), $\varphi = 1$ (stoichiometric reaction) and $\varphi = 1.1$ (fuel-rich region) are chosen as the representatives for the cases investigated in the present work. As shown by this figure, in air-firing condition, without preheating, reaction can not take place in the highly diluted and ultra-lean fuel region (i.e. $\varphi \leq 0.7$). Through our simulation, $\varphi = 0.793$ is the minimum for the methane-air HDDI configuration to trigger reaction without preheating (as shown by Fig. 2(a), when $T_{oxi}/T_0 = 1.0$ and $\varphi \leq 0.7$ there is no temperature rise). With a relatively low pre-

heating temperature (namely, $T_{oxi}/T_0 = 2.0$), combustion can be sustained stably in the fuel lean region. With a higher preheating temperature, such as $T_{oxi}/T_0 = 3.0$, stable reaction can occur even in the highly diluted region as the preheating temperature now is above the ignition temperature of methane. For some preheating temperatures, such as $T_{oxi}/T_0 = 3.0$ and 4.0, there will be an obvious peak in the temperature profile even when $\varphi = 0.5$, which implies with a high preheating temperature the heat released in the highly diluted fuel region also can generate a local "hotspot" and it is harmful to establish an even temperature distribution. With a much higher preheating temperature (e.g. $T_{oxi}/T_0 \geq 5.0$), such negative influence on forming even temperature distribution can be suppressed. In air-firing condition, the maximum temperature in the fuel-rich region is substantially higher than its fuel-lean counterpart. Consequently, if a fuel-rich scenario appears in practical operation, the fluctuation of fuel flow should be paid high attention to avoid potential safety problems.

In our previous study [9], we investigated hydrogen-air combustion in various regimes. A comparison between Fig.2 in this work and Fig. 2 in Ref.[9] indicates the composition of fuels will influence reaction structures significantly. As shown in Ref.[9], the reaction zone of hydrogen-air HDDI combustion will become thick obviously and will expand to the oxidant jet side with T_{oxi} and φ increasing. However, different from its hydrogen counterpart, the thickness of the reaction zone of methane-air HDDI combustion is nearly insensitive to T_{oxi} and φ. Such observation is important for burner design, especially for some demonstration-scale furnaces in which opposed burners were equipped[54]. This difference may result from that the diffusivity of methane is much smaller than hydrogen. Meanwhile, there are some similarities between methane-air HDDI combustion and its hydrogen counterpart. In hydrogen-air HDDI combustion, it was observed no matter whatever T_{oxi} was, the maximum temperature of reactants (T_{max}) increased with φ but the increment of T_{max} decreased against T_{oxi} [9]. This conclusion is true for its methane counter-

part. As illustrated by Fig.2, T_{max} climbs up with φ and the increasing rate of T_{max} becomes slow against T_{oxi}. It can be shown more clearly from Fig. 3. Moreover, according to Fig. 3, it can be observed that for $\varphi \leq 1.0$, T_{max} will grow up almost linearly with T_{oxi} if the reactants can be ignited. In the fuel lean region ($0.7 \leq \varphi < 1.0$), the lines are nearly parallel with each other. While in the ultra-lean and highly diluted fuel region ($\varphi < 0.7$) the lines will intersect at $T_{oxi} = 6.0$. Such observation indicates, with a high preheating temperature, if fuel supply is not sufficient, the heat released by the exothermic reactions is much smaller than the energy borne by the preheated oxidant flow. Especially in the highly diluted fuel region ($\varphi \leq 0.5$), the heat released by the exothermic reactions may not compensate heat loss, as depicted by Fig.2 (f): where a temperature peak appears when $\varphi = 0.7$, there is a temperature drop for $\varphi = 0.5$. This phenomenon does not exist when $T_{oxi} \leq 5.0$ (except the cases with $T_{oxi} \leq 2.0$ as in which reactions are not triggered). $T_{oxi} = 5.0$ perhaps is a critical temperature point for the cases investigated

in the present work as at this preheating temperature level there is no temperature rise or temperature drop within the reaction zone. Making an comparison with the data reported by Ref.[9], it can be observed that such critical temperature point depends on fuel types. As shown by Fig. 2(c) in Ref.[9], while $T_{oxi} = 5.0$ there is still a slight temperature peak in hydrogen-air HDDI combustion. The temperature rise of reactants $\Delta T = T_{max} - T_{oxi}$ is plotted by Fig. 4. Through this figure, it can be concluded that ΔT is a monotonic decreasing function of T_{oxi}, except the cases in which reaction can not be ignited (e.g. when $\varphi < 0.5$ and $T_{oxi}/T_0 < 2.0$). These features are similar with its hydrogen counterpart reported in Ref.[9] except two differences: (1) as hydrogen is more active than methane, obvious temperature rise can be observed even when $\varphi \leq 0.4$, but not for its methane counterpart; (2) the decreasing rates of ΔT in methane-air HDDI combustion and its hydrogen counterpart are different. These differences imply combustion regimes depending closely on fuel types. In Ref.[7] Cavaliere et al. assumed that the classification of

various combustion regimes might rely on fuels used. The present results can confirm their assumption.

According to Fig. 4, we can depict the map of different combustion regimes in methane-air HDDI configuration, as illustrated by Fig. 5. In Fig. 5, φ and T_{oxi} are chosen as the coordinates. The benefits to adopt them to classify different combustion regimes have been discussed in our previous work [9]. Similar with its hydrogen counterpart discussed in our previous study [9], there are five combustion regimes in methane-air HDDI combustion condition, as defined by Table 2. The detailed explanation on Table 2 is presented in Ref.[9]. Through a comparison between Fig. 5 in the present work and Fig.4 in Ref.[9], one can observe there are four obvious differences between the combustion regimes of methane-air HDDI configuration and those of its hydrogen counterpart. Firstly, the transient regime, namely the "Flameless" regime, is much narrower in methane-air HDDI combustion than its hydrogen counterpart. Especially, without preheating there is no "Flameless" regime in the former. Secondly, the zone of "No

Table 2
The classification of different combustion regimes for for methane-air HDDI combustion.

Combustion mode	Inlet conditions	Working conditions
Feedback combustion	$T_{oxi} < T_{si}$	$\Delta T > T_{si}$
HiTAC	$T_{oxi} > T_{si}$	$\Delta T > T_{si}$
Mild combustion	$T_{oxi} > T_{si}$	$\Delta T < T_{si}$
"Flameless"	$T_{oxi} < T_{si}$	$\Delta T \geq T_{si} - T_{oxi}$

Combustion" regime is larger in methane-air HDDI combustion, compared with its hydrogen counterpart. Thirdly, in methane-air HDDI combustion, the "MILD Combustion" regime exists nearly impossibly in the fuel-rich region but it is not true for its hydrogen counterpart. Finally, in methane-air HDDI combustion, the "Feedback Combustion" regime can emerge in the fuel-lean region while it is nearly impossible in its hydrogen counterpart. Consequently, in air-firing condition, compared with hydrogen, it is more complicated for methane to organize and sustain MILD combustion. More important, one should bear in mind that fuel types will influence the pathway to MILD combustion regime critically. Especially for practical furnaces where a high preheating temperature is restricted for safety reasons.

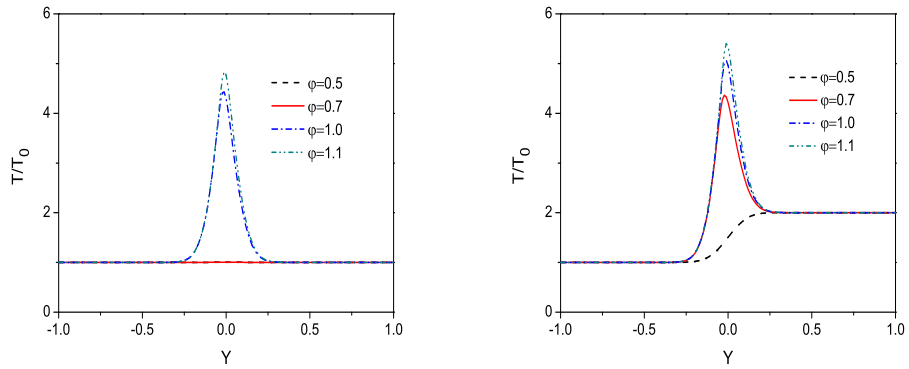

(a)

(b)

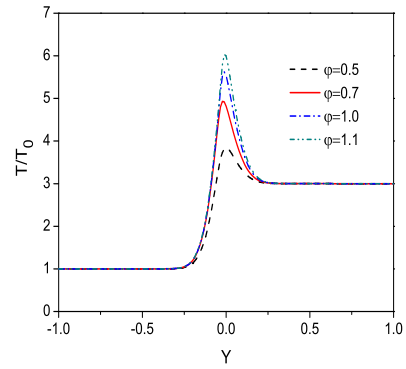

(c)

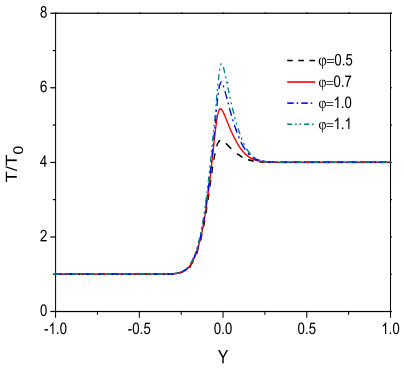

(d)

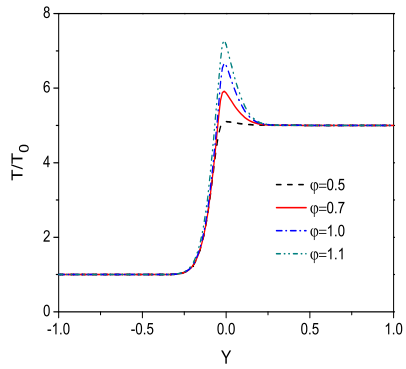

(e)

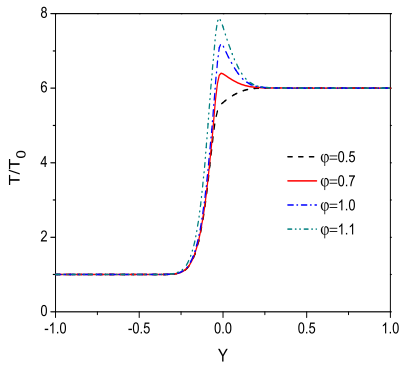

(f)

Fig. 2. Distributions of temperature with different φ along line $x = 0$ in air-firing condition: (a) $T_{oxi}/T_0 = 1$ (b) $T_{oxi}/T_0 = 2$ (c)$T_{oxi}/T_0 = 3$ (d)$T_{oxi}/T_0 = 4$ (e) $T_{oxi}/T_0 = 5$ (f) $T_{oxi}/T_0 = 6$.

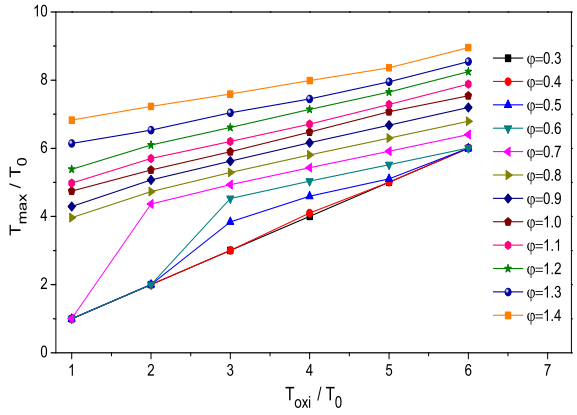

Fig. 3. Variations of maximum temperature of reactants, methane-air configuration.

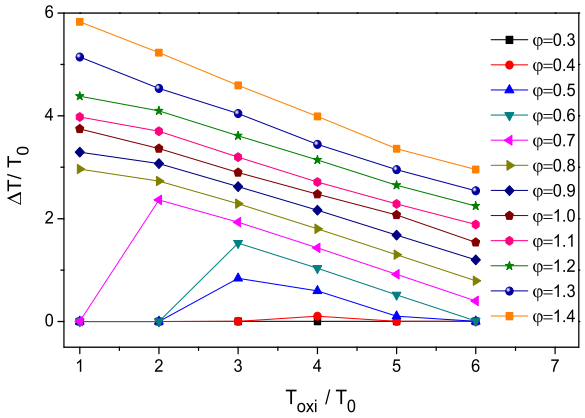

Fig. 4. Temperature rise of reactants, methane-air configuration.

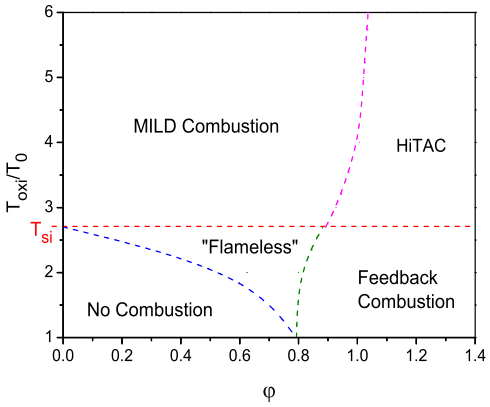

Fig. 5. Combustion regimes presented in $\varphi - T_{oxi}$ map: air-firing condition.

4.1.2 Temperature profiles in oxyfuel condition and comparison between different dilution atmosphere

Figure 6 illustrates the temperature profiles at various equivalence ratio and preheating temperature of oxidant flow in oxyfuel condition. Different from its air-firing counterpart discussed above, in oxyfuel condition, oxygen in the oxidant flow is diluted by CO_2 instead of nitrogen. As the specific heat capacity of CO_2 is bigger than air, the peak values of temperature of the reactants are much lower than those in air-firing condition (c.f. Fig. 2). Especially, without preheating, combustion can not be sustained in CO_2/O_2 atmosphere when $\varphi < 1.33$. More important, it can be observed that the reaction zone in oxyfuel condition will hardly expand with φ increasing, which results from the lower diffusive coefficients of reactants in CO_2 atmosphere. In our previous study [43], we analyzed the physical and chemical effects of CO_2 on reaction characteristics and concluded the physical effect of CO_2 played a predominant role. The present observation agrees with this conclusion. In addition, due to the large specific heat capac-

ity of CO_2, there will not appear a local "hotspot" in the highly diluted fuel region (namely $\varphi < 0.5$), no matter whatever T_{oxi} is. With a high preheating temperature, if in fuel-lean condition, the heat released by the exothermic reactions may be much smaller than the energy borne by the preheated oxidant flow, which will cause a temperature drop within the reaction zone instead of a temperature jump, as shown by Fig. 6 (e). This phenomenon also exists in its air-firing counterpart.

The maximum temperature of reactants T_{max} in oxyfuel condition is plotted in Fig. 7. According to this figure, one can observe that T_{max} is a monotonic increasing function of T_{oxi} and φ, similar with its air-firing counterpart. In addition, in the highly diluted fuel region, the lines of T_{max} with various φ almost overlap with each other as the heat released by exothermic reactions is too slight to induce temperature fluctuation, which also can be observed in its air-firing counterpart. However, their differences are obvious, too. Due to the high specific heat capacity of CO_2, local "hotspots" can be suppressed in oxyfuel condition.

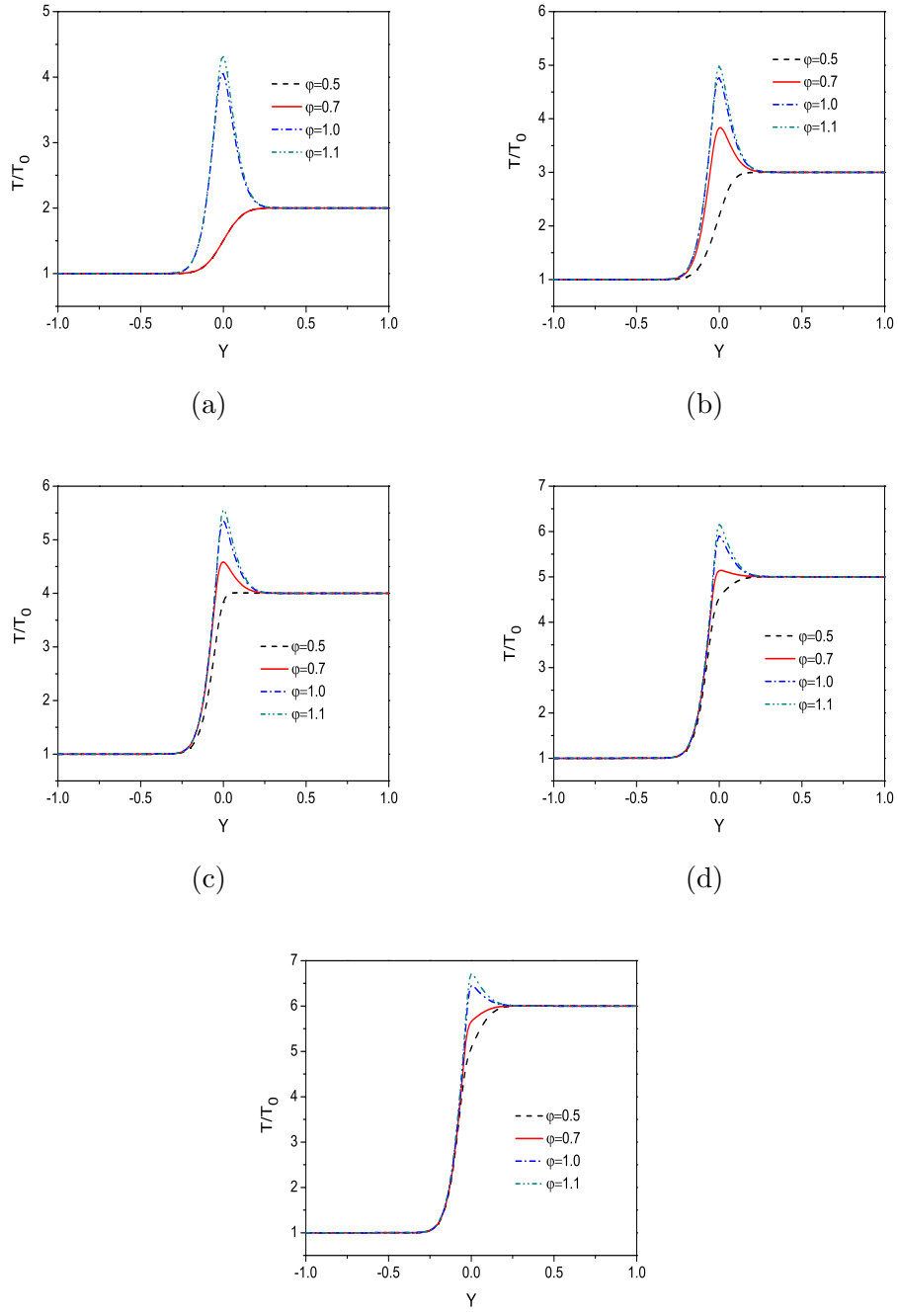

Fig. 6. Distributions of temperature with different φ along line $x = 0$ in oxyfuel condition: (a) $T_{oxi} = 2$ (b) $T_{oxi} = 3$ (c)$T_{oxi} = 4$ (d)$T_{oxi} = 5$ (e) $T_{oxi} = 6$.

For example, there is no obvious temperature jump for $\varphi = 0.6$ in oxyfuel condition but in its air-firing counterpart there will

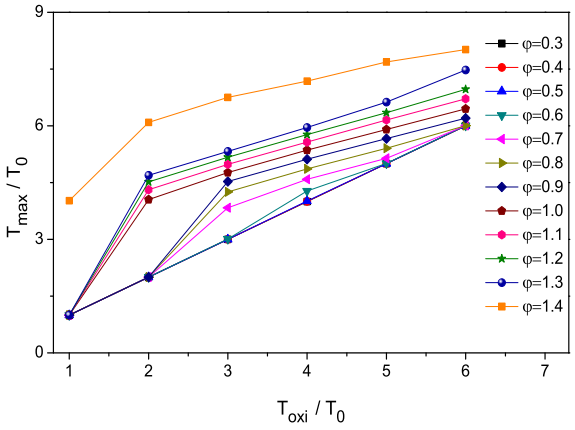

Fig. 7. Variations of maximum temperature of reactants, methane-oxyfuel configuration.

appear a significant temperature rise even when $\varphi = 0.5$. Moreover, in methane-oxyfuel HDDI combustion, T_{max} will experience a "jump" when φ increases from 1.3 to 1.4 (as illustrated by Fig. 7, the gap between the contour $\varphi = 1.3$ and the contour $\varphi = 1.4$ is obviously larger than others). On the contrary, the variation of T_{max} versus φ is "smooth" in its air-firing counterpart. Figure 8 shows the temperature rise of reactants. In oxyfuel condition, ΔT will decrease linearly against T_{oxi}, similar with its air-firing counterpart, although the decreasing speed in oxyfuel condition is slower.

With Fig. 8, the map of different combustion regimes in oxyfuel condition can be plotted, as shown by Fig. 9. Through a

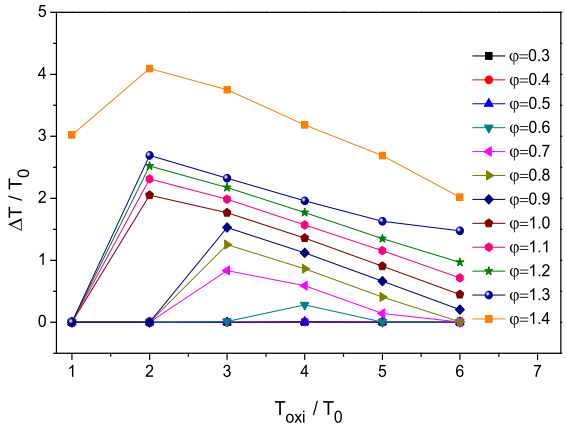

Fig. 8. Temperature rise of reactants, methane-oxyfuel configuration.

comparison between Fig. 5 and Fig. 9, some claims in previous publications can be explained straightforwardly. For instance, in Ref.[20] it was claimed that MILD combustion could be maintained more easily in CO_2/O_2 atmosphere. As shown by Fig. 9, in oxyfuel condition, the "MILD Combustion" regime occupies a larger area than in air-firing condition, so MILD combustion can be sustained over a wider operational range accordingly. It is important for practical applications because in which obvious fluctuation of concentration of reactants is inevitable. Furthermore, a theoretical explanation can be drawn to support why the best pathway to safely and effectively organize the "MILD Combustion" regime in oxyfuel condition (namely the so-called MILD oxyfuel combustion) is to start from air-firing condtion. In

our previous experimental efforts [54], we drew such conclusion empirically without a clear theoretical support. As illustrated by Fig. 9, compared with its air-firing counterpart (c.f. Fig. 5) the "No Combustion" regime also occupies a larger area in oxyfuel condition, which expands even to the fuel-rich region. It implies that the possibility of extinction is very high if we run a cold furnace in CO_2/O_2 atmosphere at the beginning. However, it is relatively easy to guarantee stable combustion in air-firing condition, even in the fuel-lean region. For practical applications, considering safety reasons, the preheating temperature is restricted not too high. To meet this restriction, in the first stage we should operate a furnace to reach the "Feedback Combustion" regime in air-firing condition. Then we can shift to oxyfuel condition through replacing air by CO_2/O_2. The combustion will switch to the "Flameless" regime automatically (please keep in mind that a part of the "Feedback Combustion" regime in air-firing condition overlaps with that of the "Flameless" regime in oxyfuel condition as the "Flameless" regime expands in oxyfuel condition).

Finally, we may approach to the "MILD Combustion" regime through further preheating the oxidant flow by hot exhaust gas. According to the maps depicted in Figs. 5 and 9, one also can identify the crucial step in the above processes is the transition from the "Feedback Combustion" regime in air-firing condition to the "Flameless" regime in oxyfuel condition as this step may meet the hazard of extinction in an industrial furnace. It is well-known in a practical furnace heat loss is inevitable. As shown in our previous work [9], the critical condition that the "Flameless" regime can be sustained is that the heat released by exothermic reactions could accumulate to ignite the fresh reactants as in the "Flameless" regime the preheating temperature of the oxidant flow is lower than the ignition temperature. If the heat loss of a furnace overweighs the heat accumulation, the "Flameless" regime will collapse and it is impossible to approach to the "MILD combustion" regime. The furnace will fall into the "No Combustion" regime and a safety accident has to be faced. With these maps, one may design another pathway to reach MILD oxyfuel

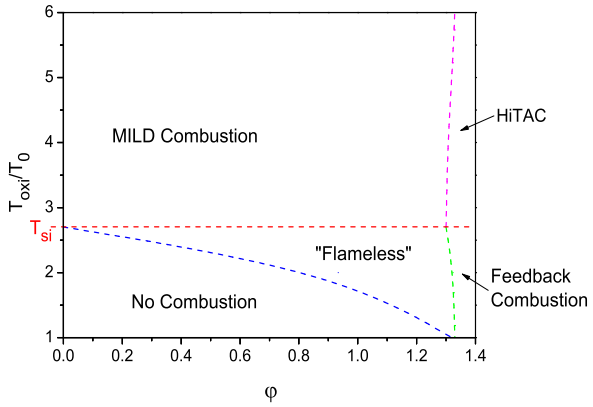

Fig. 9. Combustion regimes presented in $\varphi - T_{oxi}$ map: oxyfuel combustion condition.

combustion through crossing the "HiTAC" regime. Unfortunately, such pathway is not cost-effective for practical applications as the requirements of material for furnace construction and the consumption of fuels for industrial operation are too high. Moreover, as discussed below, along a transition pathway crossing the boundary between the "HiTAC" regime and the "MILD Combustion" regime, one has to pay great attention on the abrupt change of temperature distribution and its negative influence on combustion stability.

In addition, through the present work, it is found that, for methane oxyfuel HDDI combustion, there is a critical value of φ. As illustrated by Fig. 7, the critical value is $\varphi \approx 1.3$. A small fluctuation

around the critical value will cause abrupt changes of temperature profiles and reaction structures, as shown by Fig. 7. Being reflected on the map of combustion regimes, it corresponds with a sharp-cliff-like boundary between combustion regimes (e.g. the boundary between the "MILD Combustion" regime and the "HiTAC" regime in Fig. 9). In hydrogen HDDI combustion, there is not a critical vale of φ (i.e. any small fluctuation of hydrogen concentration will not cause an abrupt change of temperature profiles and reaction structures, as shown by Fig.3 in Ref.[9]), so the boundary between the "MILD Combustion" regime and the "HiTAC" regime looks like a gentle slope, as illustrated by Fig.4 in Ref.[9]. It is a new interesting finding that there is a relationship between a sharp-cliff-like boundary in the map and a critical vale of φ in combustion. This finding may be very useful for practical operation. For example, with the maps shown by Fig.9 at hand, if one observe a methane-fed combustion system is run at a state near the sharp-cliff-like boundary between combustion regimes, for safety it is reasonable to act immediately to

escape the state, avoiding potentially abrupt changes due to a small fluctuation. An open question emerges: whether this conclusion can be extended to other fuels? Further investigation is desired to answer it. If so, the purposes of a combustion regime classification map can be extensively expanded, not only to be used to design a feasible pathway to reach a destination combustion regime, but also to be adopted as an safety indicator for practical operation.

4.2 Influences of fuel type and dilution atmosphere on entropy generation in various combustion regimes

The above-mentioned discussions all are based on the first law of thermodynamics. During the past decades, entropy generation analysis stemmed from the second law of thermodynamics has become a powerful tool for combustion optimization [57,58]. However, a comprehensive anslysis on the effects of fuel types and dilution atmosphere on entropy generation in various combustion regimes is absent yet. In this subsection entropy generation

analysis is firstly carried out for methane-air HDDI combustion. Then a comparison is made with the results presented in our previous publication [9] to reveal the influences of different fuels on entropy generation in various combustion regimes. In succession, a comparison between methane-air HDDI combustion and methane-oxyfuel HDDI combustion is conducted to show the effects of different dilution atmosphere.

4.2.1 Entropy generation in air-firing condition

Figure 10 illustrates the variation of S_{total} with different φ in air-firing condition, where the cases with $T_{oxi} = 1, 2, 6$ are chosen as the representatives. Although S_{total} is always a monotonic increasing function of φ, the increasing rates in various combustion regimes are quite different. In the "No Combustion" regime, S_{total} is slight as where the only contributors to exergy loss are the irreversibility due to fluid friction and due to mass transfer. In both the "Flameless" regime and the "MILD Combustion" regime, S_{total} grows relatively slowly with φ. While in the "Hi-

TAC" regime or the "Feedback Combustion" regime, S_{total} rises sharply. What should be mentioned is the increasing rate of S_{total} in the "Feedback Combustion" regime is faster than that in the "HiTAC" regime. In the fuel-lean region, no matter in which combustion regime, a higher preheating temperature will cause more irreversibility because when fuel is insufficient a higher preheating temperature can enhance chemical reaction as well as temperature difference. Accordingly, the irreversibility due to chemical reaction and heat transfer will be intensified. However, in the "HiTAC" regime, a higher T_{oxi} can suppress irreversibility generation, as shown in Fig.11. This observation indicates that in the "HiTAC" regime the irreversibility due to heat transfer becomes the predominant contributor to exergy loss, as a higher T_{oxi} can reduce the temperature difference near the reaction zone, which can decrease the irreversibility due to heat transfer accordingly. Furthermore, one can conclude that in the fuel-lean region, no matter in which combustion regime, the irreversibility due to chemical reaction is the predominant contributor to exergy

loss. These findings are helpful to optimize a combustion system as the first and crucial step for combustion system optimization is to identify the dominant contributors to entropy generation [58,59].

Compared with the results presented in Ref.[9] where hydrogen-air HDDI combustion was investigated, it can be observed that there are some common features of entropy generation between hydrogen and methane in air-firing condition: (1) S_{total} is always a monotonic increasing function of φ (Fig.10 in Ref. [9]); (2) in the "HiTAC" regime the irreversibility due to heat transfer is the major contributor to exergy loss (Fig.12 in Ref. [9]). However, from the viewpoint of entropy production analysis, the differences between them are also obvious. Firstly, as shown by Fig.10 in Ref. [9], S_{total} grows almost linearly with φ in hydrogen-air HDDI combustion. Moreover, the lines in that figure are nearly parallel with each other. It implies that for hydrogen-air HDDI combustion the increasing rates of S_{total} in all combustion regimes are nearly the same and insensitive to T_{oxi}. However, as

shown by Fig.10 in the present work, it can be observed that for its methane counterpart the influence of combustion regimes on variation of S_{total} is complicated and the variation speed of S_{total} depends closely on T_{oxi}. Secondly, as illustrated by Fig.12 in Ref. [9], for hydrogen-air HDDI combustion in the fuel-lean region, the major contributor to entropy generation is not always the irreversibility due to chemical reaction. In the "Flameless" regime, the irreversibility due to chemical reaction occupies a great share, similar with its methane counterpart. However, in the "MILD Combustion" regime, the irreversibility due to chemical reaction and that due to heat transfer compete with each other. The major contributor to exergy destroy depends closely on T_{oxi}. It is quite different form its methane counterpart. Thirdly, recently Soroudi and Ghafourian [60] investigated entropy generation in the "HiTAC" regime and "MILD Combustion" regime of methane-air HDDI combustion and they concluded that the intensity of irreversibility generation, namely the maximum value of local entropy generation number S_{max}, would decrease as

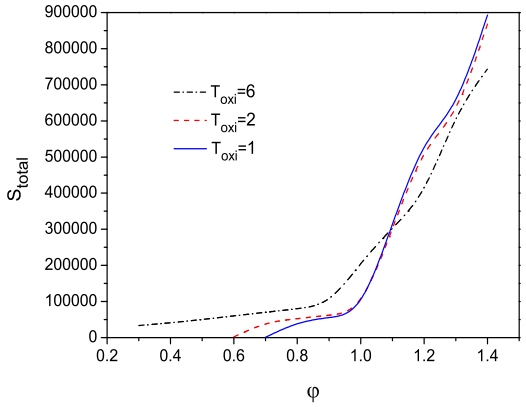

Fig. 10. Variation of S_{total} with different φ and T_{oxi} in air-firing condition.

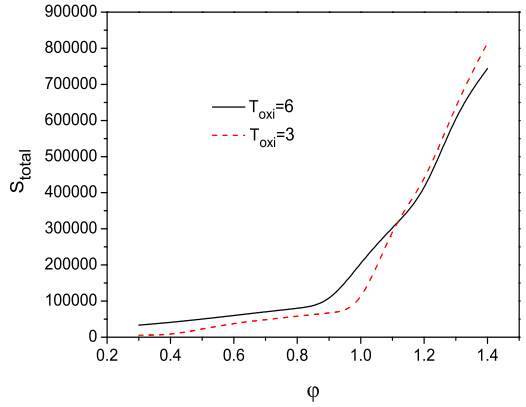

Fig. 11. Variation of S_{total} with different φ and T_{oxi} in "MILD Combustion" and "HiTAC" regimes.

the dilution becomes more intense. Fig.12 in the present work agrees well with their conclusion. In addition, The present results can demonstrate this conclusion can hold water for all combustion regimes in methane-air HDDI condition. However, as shown by Fig.10 in Ref. [9], this conclusion is not always true for its hydrogen counterpart.

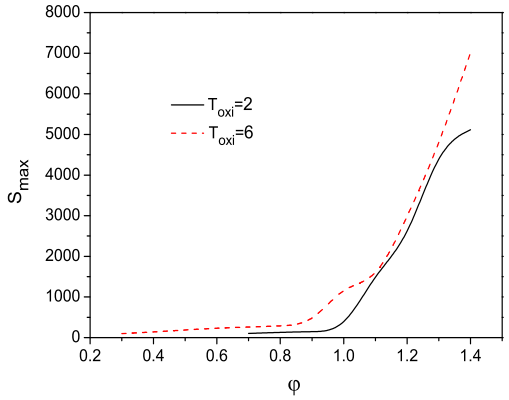

Fig. 12. Variation of S_{max} with different φ and T_{oxi}.

4.2.2 Entropy generation in oxyfuel condition

The variation of S_{total} in oxyfuel condition is depicted by Fig.13. It can be observed that S_{total} is always a monotonic increasing function of φ in all combustion regimes although the increasing rates in various regimes are different. In the "No Combustion" regime, S_{total} is slight as where the only contributors to exergy loss are the irreversibility due to fluid friction and due to mass transfer. In both the "Flameless" regime and the "MILD Combustion" regime, S_{total} grows relatively slowly with φ. While in the "HiTAC" regime or the "Feedback Combustion" regime, S_{total} climbs up sharply. These features in oxyfuel condition are the same as its air-firing counterpart. However, the differences

between them are also obvious. Firstly, in air-firing condition, S_{total} in the "Feedback Combustion" regime will exceed that in the "HiTAC" regime while in oxyfuel condition it is not the truth. Secondly, as shown by Fig.14, in the "HiTAC" regime, S_{total} with a higher T_{oxi} is always larger than that with a lower T_{oxi}. It is completely contrary to its air-firing counterpart. According to Figs.13-14, it can be concluded that in oxyfuel condition, in all combustion regimes, a higher T_{oxi} corresponds a bigger S_{total}. This conclusion implies that in oxyfuel condition the irreversibility due to chemical reaction is always the major contributor to exergy destroy, no matter in which combustion regime. This feature is different from its air-firing counterpart where the irreversibility due to chemical reaction and that due to heat transfer are competitive. Finally, S_{total} in oxyfuel condition is much lower than its air-firing counterpart because temperature jump near the reaction zones (c.f. Figs. 2 and 6), as well as reaction rates (the details please refer to our previous publications [43,51]), is smaller in CO_2/O_2 atmosphere. Consequently, the irreversibility due

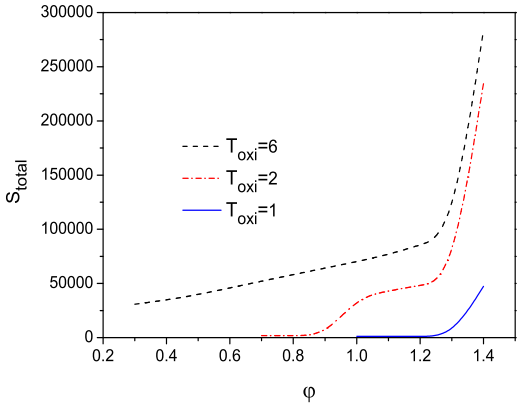

Fig. 13. Variation of S_{total} with different φ and T_{oxi} in oxyfuel condition.

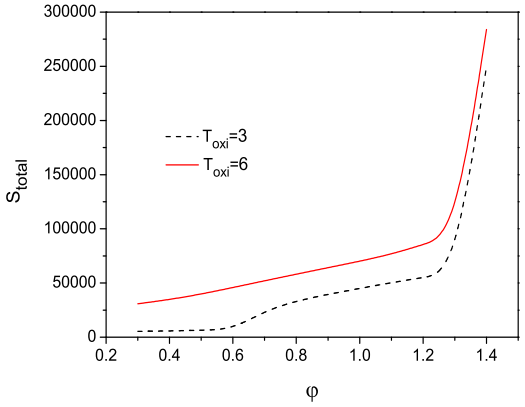

Fig. 14. Variation of S_{total} with different φ and T_{oxi} in "MILD Combustion" and "HiTAC" regimes.

to chemical reaction and that due to heat transfer both descend.

Figure 15 illustrates the variation of S_{max} with different φ and T_{oxi}. Through this figure, one can observe that the intensity of irreversibility generation descends as the dilution become more intense. Namely, the conclusion drawn in air-firing condition[60] can be extended to its oxyfuel counterpart. It also can be ob-

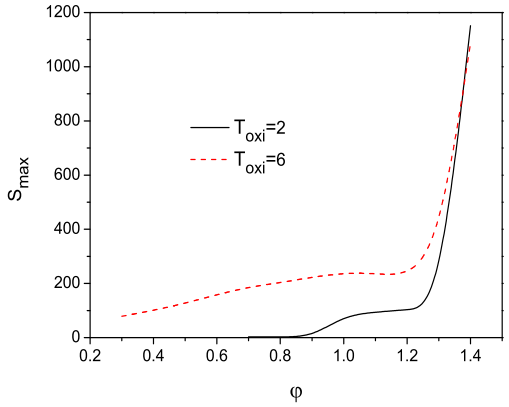

Fig. 15. Variation of S_{max} with different φ and T_{oxi}.

served that S_{max} in oxyfuel condition is much smaller than its air-firing counterpart and the reason has been given above. A difference between them is illustrated by Fig.15. In the figure, one can observe that the gap between the lines becomes to diminish in the "HiTAC" regime. It implies in the "HiTAC" regime of oxyfuel condition the irreversibility due to heat transfer becomes as important as that due to chemical reaction.

Finally, according to Figs.10, 12, 13 and 15, one also can conclude that a transition pathway from the "HiTAC" regime to the "MILD Combustion" (or MILD oxyfuel) regime is not economical, from the viewpoint of the second thermodynamic-law, as more entropy (namely exergy destroy) will be generated a-

long such pathway. The most economical pathway is crossing the "Flameless" regime, which agrees with the above result obtained from the viewpoint of the first thermodynamic-law. Consequently, the first and second thermodynamic-law analyses on the maps of combustion regimes both can provide a consistent theoretical guide on how to design an efficient way to establish and to sustain "MILD Combustion" (or MILD oxyfuel) regime, from the standpoint of safety and of cost, respectively.

5 Conclusion

The idea of MILD oxyfuel combustion has attracted increasing attention as a clean approach to utilize fossil fuels. However, it is impossible to establish MILD oxyfuel combustion directly. In the present study, we try to address this challenge with the aid of combustion regime maps. The major findings of the present investigation can be summarized as:

(1) Through a comparison between the combustion regime map-

s, an efficient pathway to establish and sustain MILD oxyfuel combustion can be determined, which agrees with our empirical experiences.

(2) Through the present work, it can be observed that the effects of fuel type and dilution atmosphere on combustion regime classification are significant.

(3) With the aid of the second thermodynamic-law analysis, the major contributors to exergy loss can be identified clearly.

(4) The purposes of a map of combustion regime classification are extensively expanded by this work. Besides being used to design a pathway to establish MILD combustion, the map also can be adopted as a safety indicator for combustion operation.

Acknowledgments

This work has received funding from the Universidad Carlos III de Madrid, the European Unions Seventh Framework Programme for research, technological development and demonstration under

grant agreement No. 600371, el Ministerio de Economa y Competitividad (COFUND2014-51509), el Ministerio de Educacin, cultura y Deporte (CEI-15-17) and Banco Santander. We also acknowledge the support from the British Newton Alumni Fellowship Scheme, the National Natural Science Foundation of China (Grant No. 51176061).

References

[1] IEA (2015), World Energy Outlook Special Report: Energy and Climate Change, OECD/IEA, Paris.

[2] Cavaliere A, de Joannon M. Mild Combustion. Progress in Energy and Combustion Science 2004; 30: 329-366.

[3] Buhre BJP, Elliott LK, Sheng CD, Gupta RP, Wall TF. Oxy-fuel combustion technology for coal-fired power generation. Progress in Energy Combust Science 2005;31:283-307.

[4] Cavigiolo A, Galbiati M A, Effuggi A, Gelosa D, Rota R. Mild combustion in a laboratory-scale apparatus. Combustion Science and Technology 2003;175:1347-1367

[5] Galbiati MA, Cavigiolo A, Effuggi A, Gelosa D, Rota R. Mild combustion for fuel-NOx reduction. Combustion Science and Technology 2004;176:1035-1054

[6] De Joannon M, Matarazzo A, Sabia P, Cavaliere A. MILD combustion in homogeneous charge diffusion iginition (HCDI) regime. Proceedings of the Combustion Institute. 2007;:3409-3416.

[7] De Joannon M, Sabia P, Sorrentino G, Cavaliere A. Numerical study of mild combustion in hot diluted diffusion ignition (HDDI) regime. Proceedings of the Combustion Institute. 2009;32:3147-3154.

[8] de Joannon M, Sorrentino G, Cavaliere A. MILD combustion in diffusion-controlled regimes of Hot Diluted Fuel. Combustion and Flame 2012;159:1832-1839

[9] Chen S, Mi J, Liu H, Zheng C. First and second thermodynamic-law analyses of hydrogen-air counter-flow diffusion combustion in various combustion modes. International Journal of Hydrogen Energy 2012;37:5234-5245

[10] Wang F, Mi J, Li P. Combustion Regimes of a Jet Diffusion Flame in Hot Co-flow. Energy Fuels 2013;27:3488-3498

[11] Evans MJ, Medwell PR, Wu H, Stagni A, Ihme M. Classification and lift-off height prediction of non-premixed MILD and autoignitive flames. Proceedings of the Combustion Institute (in press) doi:10.1016/j.proci.2016.06.013

[12] Szego GG, Dally BB, Nathan GJ. Operational characteristics of a parallel jet MILD combustion burner system. Combustion and Flame 2009;156: 429-438

[13] Dally BB, Karpetis AN, Barlow RS. Structure of turbulent non-premixed jet flames in a diluted hot coflow. Proceedings of the Combustion Institute 2002;29: 1147-1154

[14] Weber R, Smart JP, Kamp W. On the (MILD) combustion of gaseous, liquid, and solid fuels in high temperature preheated air. Proceedings of the Combustion Institute 2005;30:2623-2629.

[15] Effuggi A, Gelosa D, Derudi M, Rota R. Mild combustion of methane derived fuel mixtures: natural gas and biogas. Combustion Science and Technology 2008;180: 481-493.

[16] Tu Y, Liu H, Chen S, Liu Z, Zhao H, Zheng C. Effects of furnace chamber shape on the MILD combustion of natural gas. Applied Thermal Engineering 2015;76:64-75

[17] Noor MM, Wandel AP, Yusaf T. MILD Combustion: The Future for Lean and Clean Combustion Technology. International Review of Mechanical Engineering 2014;8:251-257

[18] Kim JP, Schnell U, Scheffknecht G. Comparison of Different Global Reaction Mechanisms for MILD Combustion of Natural Gas. Combustion Science and Technology 2008;180:565-592

[19] Wang L, Chen S, Liu Z, Zheng CG. Comparison of Different Global Combustion Mechanisms for Use in CFD Modeling under Hot and Diluted Oxidation Condition. Combustion Science and Technology 2012;184:259-276

[20] Chen S, Zheng CG. Counterflow diffusion flame of hydrogen-enriched biogas under MILD oxy-fuel condition. International Journal of Hydrogen Energy 2011;36:15403-15413.

[21] Hamdi M, Benticha H, Sassi M. Evaluation of reduced chemical kinetic

mechanisms used for modeling mild combustion for natural gas. Thermal Science 2009;13: 131-137

[22] Galletti C, Parente A, Derudi M, Rota R, Tognotti L. Numerical and experimental analysis of NO emissions from a lab-scale burner fed with hydrogen-enriched fuels and operating in MILD combustion. International Journal of Hydrogen Energy 2009;34: 8339-8351

[23] Mardani A, Tabejamaat S. NOx Formation in H2-CH4 Blended Flame Under MILD Conditions. Combustion Science and Technology 2012;184:995-1010

[24] Li P, Wang F, Mi J, Dally BB, Mei Z, Zhang J, Parente A. Mechanisms of NO formation in MILD combustion of CH4/H2 fuel blends. International Journal of Hydrogen Energy 2014;39:19187-19203

[25] Loffler G, Sieber R, Harasek M, Hofbauer H, Hauss R, Landauf J. NOx formation in natural gas combustion-a new simplified reaction scheme for CFD calculations. Fuel 2006;85: 513-523

[26] Galletti C, Ferrarotti M, Parente A, Tognotti L. Reduced NO formation models for CFD simulations of MILD combustion. International Journal of Hydrogen Energy 2015;40: 4884-4897

[27] Bozzelli JW, Dean AM. O+NNH: A possible new route for NOX formation in flames. International Journal of Chemical Kinetics 1995;27:1097-1109

[28] Konnov A, Colson G, Ruyck JD. The new route forming NO via NNH. Combustion and Flame 2000;121(3):548-550

[29] Nicolle A, Dagaut P. Occurrence of NO-reburning in MILD combustion evidenced via chemical kinetic modeling. Fuel 2006;85:2469-2478

[30] Parente A, Galletti C, Tognotti L. A simplified approach for predicting NO formation in MILD combustion of CH4-H2 mixtures. Proceedings of the Combustion Institute 2011;33: 3343-3350

[31] Fortunato V, Galletti C, Tognotti L, Parente A. Influence of modelling and scenario uncertainties on the numerical simulation of a semi-industrial flameless furnace. Applied Thermal Engineering 76 (2015), 324- 334.

[32] Mi J, Li P, Dally BB, Craig RA. Importance of initial momentum rate and air-fuel premixing on moderate or intense low oxygen dilution (MILD) combustion in a recuperative furnace. Energy and Fuel. 2009;23:5349-5356.

[33] Mardani A, Tabejamaat S, Ghamari M. Nuerical study of molecular diffusion in the MILD combustion regime. Combustion Theory and Modelling. 2010; 14:747-774

[34] Aminian J, Galletti C, Tognotti L. Extended EDC local extinction model accounting finite-rate chemistry for MILD combustion. Fuel 2016;165:123-133

[35] Parente A, Malik MR, Contino F, Cuoci A, Dally BB. Extension of the Eddy Dissipation Concept for turbulence/chemistry interactions to MILD combustion. Fuel 2016;163:98-111

[36] Hosseini SE, Wahid MA. Enhancement of exergy efficiency in combustion systems using flameless mode. Energy Conversion and Management 2014; 86: 1154-1163

[37] Hosseini SE, Bagheri G, Wahid MA. Numerical investigation of biogas flameless combustion. Energy Conversion and Management 2014;81:41-50

[38] Budzianowski WM. An oxy-fuel mass-recirculating process for H_2 production with CO_2 capture by autothermal catalytic oxyforming of methane. International Journal of Hydrogen Energy 2010;35:7454-7469

[39] Toftegaard MB, Brix J, Jensen PA, Glarborg P, Jensen AD. Oxy-fuel combustion of solid fuels. Progress in Energy and Combustion Science 2010;36:581-625

[40] Krishnamurthy N, Paul PJ, Blasiak W. Studies on low-intensity oxy-fuel burner. Proceedings of the Combustion Institute 2009;32:3139-3146

[41] Khare SP, Wall TF, Farida AZ, Liu Y, Moghtaderi B, Gupta RP. Factors influencing the ignition of flames from air-fired swirl pf burners retrofitted to oxy-fuel. Fuel 2008;87:1042-1049

[42] Andersen J, Rasmussen CL, Giselsson T, Glarborg P. Global Combustion Mechanisms for Use in CFD Modeling under Oxy-Fuel Conditions. Energy Fuels, 2009;23:1379-1389

[43] Wang L, Liu Z, Chen S, Zheng C, Li J. Physical and Chemical Effects of CO2 and H2O Additives on Counterflow Diffusion Flame Burning Methane. Energy Fuels 2013;27:7602-7611

[44] Pak PS, Lee YD, Ahn KY. Characteristics and economic evaluation of a power plant applying oxy-fuel combustion to increase power output and decrease CO_2 emission. Energy 2010;35:3230-3238.

[45] Borgert KJ, Rubin ES. Oxyfuel Combustion: Technical and Economic Considerations for the Development of Carbon Capture from Pulverized Coal Power Plants. Energy Procedia 2013;37:1291-1300

[46] Normann F., K Andersson, B Leckner, Johnsson F. Emission control of nitrogen oxides in the oxy-fuel process. Progress in Energy and Combustion Science 2009;35:385-397

[47] Chen L, Yong SZ, Ghoniem AF. Oxy-fuel combustion of pulverized coal: Characterization, fundamentals, stabilization and CFD modeling. Progress in Energy and Combustion Science 2012;38:156-214

[48] Yin C, Yan J. Oxy-fuel combustion of pulverized fuels: Combustion fundamentals and modeling. Applied Energy 2016;162:742-762

[49] Lockwood T. Developments in oxyfuel combustion of coal, CCC/240 2014

[50] Li P, Dally BB, Mi J, Wang F. MILD oxy-combustion of gaseous fuels in a laboratory-scale furnace. Combust Flame 2013;160:933-946.

[51] Liu Y, Chen S, Yang B, Liu K, Zheng C. First and second thermodynamic-law comparison of biogas MILD oxy-fuel combustion moderated by CO_2 or H_2O. Energy Conversion and Management 2015;106:625-634.

[52] Tu Y, Liu H., Chen S, Liu Z, Zhao H, Zheng C. Numerical study of combustion characteristics for pulverized coal under oxy-MILD operation. Fuel Processing Technology 2015;135: 80-90

[53] Mardani A, Ghomshi AF. Numerical study of oxy-fuel MILD (moderate or intense low-oxygen dilution combustion) combustion for CH_4-H_2 fuel. Energy

2016;99:136-151

[54] Li P, Mi J, Dally BB, Wang F, Wang L, Liu Z, Chen S, Zheng C. Progress and recent trend in MILD combustion. Sci China Technol Sci 2011;54:255-269.

[55] Chen S, Liu Z, Zhang C, He Z, Tian Z, Shi B. and Zheng C.G. A novel coupled lattice Boltzmann model for low Mach number combustion simulation. Applied Mathematics and Computation 2007;193: 266-284.

[56] Chen S, Li J, Han HF, Liu ZH, Zheng CG. Effects of hydrogen addition on entropy generation in ultra-lean counter-flow methane-air premixed combustion. Int J Hydrogen Energy 2010;35:3891-3902.

[57] A. Sciacovelli, V. Verda, E. Sciubba. Entropy generation analysis as a design tool-A review. Renewable and Sustainable Energy Reviews 2015;43: 1167-1181

[58] H.R. Arjmandi, E. Amani. A numerical investigation of the entropy generation in and thermodynamic optimization of a combustion chamber. Energy 2015;81: 706-718

[59] Jiang D, Yang W, Teng J. Entropy generation analysis of fuel lean premixed CO/H2/air flames. International Journal of Hydrogen Energy, 2015; 40:5210-5220

[60] Soroudi MA, Ghafourian A. Entropy Generation and Exergy Loss in Natural Gas Mild Combustion Process. Processes and Technologies for a Sustainable Energy 2010; doi : 10.4405/ptse2010.P1.1.